

Supporting Information

Ultra-high selectivity COF-based membranes for biobutanol production

Hongwei Fan,^{‡a} Yunfeng Xie,^{‡b} Jiachen Li,^c Li Zhang,^c Qiyu Zheng^{*b} and Guojun Zhang^{*a}

^aBeijing Key Laboratory for Green Catalysis and Separation, College of Environmental and Energy Engineering, Beijing University of Technology, 100 Ping Le Yuan, Chaoyang District, Beijing 100124, PR China

E-mail: zhanggj@bjut.edu.cn

^bBeijing National Laboratory for Molecular Sciences, CAS Key Laboratory of Molecular Recognition and Function, Institute of Chemistry, Chinese Academy of Sciences, Beijing, 100190, PR China

E-mail: zhengqy@iccas.ac.cn

^cDepartment of Chemistry, Zhejiang Sci-Tech University, Hongzhou 310018, PR China

[‡] Hongwei Fan and Yunfeng Xie contributed equally to this article.

Contents

S1. Materials

S2. Synthesis of hydrazone-based COFs materials

S2.1. Synthesis of COF-42 materials

S2.2. Synthesis of diethyl 2,5-dihydroxyterephthalate

S2.3. Synthesis of diethyl 2,5-diisopropoxyterephthalate

S2.4. Synthesis of diethyl 2,5-dipropoxyterephthalate

S2.5. Synthesis of diethyl 2,5-dibutoxyterephthalate

S2.6. Synthesis of 2,5-diisopropoxyterephthalohydrazide

S2.7. Synthesis of 2,5-dipropoxyterephthalohydrazide

S2.8. Synthesis of 2,5-dibutoxyterephthalohydrazide

S2.9. Synthesis of COF-X15, COF-X20 and COF-X21

S3. Compatibility and crosslinking density characterization

S4. MD simulation method

S4.1. Membrane model construction

S4.2. Simulation details

S5. Supplementary Figures (Fig. S1 to Fig. S31)

S6. Supplementary Tables (Table S1 to Table S2)

References (S1-S45)

S1. Materials

Hydroxyl-PDMS with a viscosity of 20000 mPa·s was purchased from China Bulestar Chengrand Chemical Co., Ltd. Tetraethoxysilane (TEOS), *n*-heptane, dibutyltin dilaurate (DBTDL), ethanol, acetone and *n*-butanol were purchased from Beijing Chemical Factory. All chemicals were of analytical grade and were used without further purification. Flat-sheet PSf ultrafiltration membranes with a nominal molecular weight cutoff of 20000 (PSf-20) were supplied by Sepro Membranes. Ultrapure water was prepared by using an RU water purification system (RiOs16, Millipore).

S2. Synthesis of hydrazone-based COFs materials

S2.1. Synthesis of COF-42 materials

1,3,5-benzenetricarbaldehyde, 2,5-diethoxy-terephthalohydrazide and COF-42 materials were synthesized according to the reported methods^{S1}. Dioxane was re-distilled from sodium. All other starting materials and solvents, if not specially mentioned, were obtained from commercial suppliers and used without further purification.

S2.2. Synthesis of diethyl 2,5-dihydroxyterephthalate

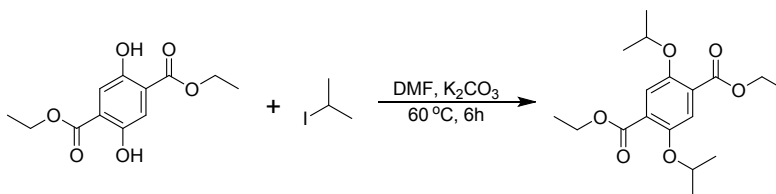


2.5 g (12.6 mmol) 2,5-dihydroxyterephthalic acid was put into a 100 ml two neck bottle, then 60 ml anhydrous EtOH was added under nitrogen atmosphere followed with 1.5 ml conc. H₂SO₄ by dropwise. Then the mixture was heated to reflux for 48 hours to complete the reaction. When cooled to room temperature, needle crystal was appeared. The titled compound was collected after filtration, washed with cool EtOH and dried in vacuum under room temperature, as a light yellow compound (2.6 g, 81%).

¹H NMR (400 MHz, CDCl₃): δ (ppm) 10.14 (s, 2H), 7.48 (s, 2H), 4.42 (q, J = 7.1 Hz, 4H), 1.42 (t, J = 7.1 Hz, 6 H).

¹³C NMR (100 MHz, CDCl₃): δ (ppm) 169.3, 153.1, 118.7, 117.9, 62.3, 14.3.

S2.3. Synthesis of diethyl 2,5-diisopropoxyterephthalate

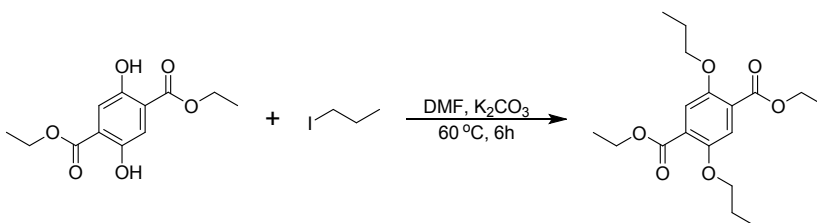


508 mg (2 mmol) diethyl 2,5-dihydroxyterephthalate, 1660 mg (12 mmol) K₂CO₃ and 5ml DMF were put into a 25 ml two neck bottle, then 220 μ l (2.2 mmol) 2-iodopropane was added into the reaction drop wise. Then the mixture was heated to 60 °C for 6 hours to complete the reaction. When cooled to room temperature, the reaction was diluted with acetic ether, filtrated and washed with acetic ether, then washed with water and brine. The organic layer was collected and dried with Na₂SO₄, and concentrated, titled compound was collected without further purification (603 mg, 89%).

¹H NMR (400 MHz, CDCl₃): δ (ppm) 7.33 (s, 2H), 4.51 (m, J = 6.1 Hz, 2H), 4.36 (q, J = 7.1 Hz, 4H), 1.38 (t, J = 7.1 Hz, 6H), 1.33 (d, J = 6.1 Hz, 12H).

¹³C NMR (100 MHz, CDCl₃): δ (ppm) 166.4, 150.8, 126.6, 119.5, 73.1, 61.4, 22.3, 14.5.

S2.4. Synthesis of diethyl 2,5-dipropoxyterephthalate

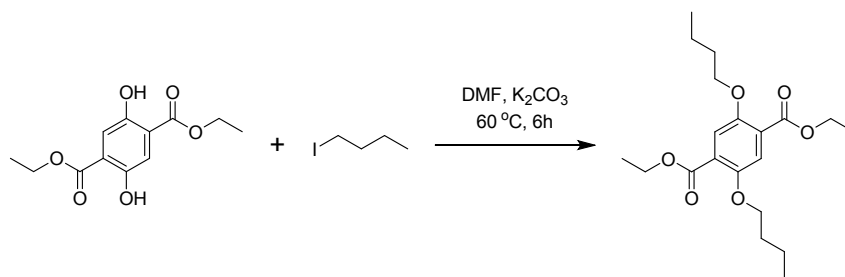


According to the method^{S1} described above by using 1-iodopropane as start material, the titled compound was collected with a yield of 85%.

¹H NMR (400 MHz, CDCl₃): δ (ppm) 7.34 (s, 2H), 4.37 (q, J = 7.2 Hz, 4H), 3.97 (t, J = 6.4 Hz, 4H), 1.89 – 1.75 (m, 4H), 1.38 (t, J = 7.1 Hz, 6H), 1.05 (t, J = 7.4 Hz, 6H).

¹³C NMR (100 MHz, CDCl₃): δ (ppm) 166.3, 151.9, 124.9, 116.8, 71.6, 61.5, 22.9, 14.5, 10.7.

S2.5. Synthesis of diethyl 2,5-dibutoxyterephthalate

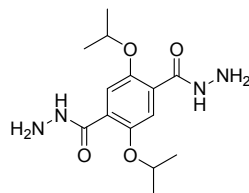


According to the method^{S1} described above by using 1-iodobutane as start material, the titled compound was collected with a yield of 91%.

¹H NMR (400 MHz, CDCl₃): (ppm) δ 7.34 (s, 2H), 4.37 (q, $J = 7.2$ Hz, 4H), 4.00 (t, $J = 6.4$ Hz, 4H), 1.78 (m, 4H), 1.59 – 1.42 (m, 4H), 1.38 (t, $J = 7.4$, 6H), 0.97 (t, $J = 7.4$ Hz, 6H).

¹³C NMR (100 MHz, CDCl₃): (ppm) δ 166.4, 151.9, 124.9, 116.8, 69.8, 61.5, 31.6, 19.4, 14.5, 14.0.

S2.6. Synthesis of 2,5-diisopropoxyterephthalohydrazide

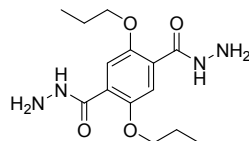


According to the reported method^{S1} by using diethyl 2,5-diisopropoxyterephthalate as starting material, the titled compound was collected with a yield of 71%.

¹H NMR (400 MHz, CDCl₃): (ppm) δ 9.25 (s, 2H), 7.84 (s, 2H), 4.80 (hept, $J = 6.1$ Hz, 2H), 4.17 (d, $J = 4.0$ Hz, 4H), 1.41 (d, $J = 6.0$ Hz, 12H).

¹³C NMR (100 MHz, CDCl₃): (ppm) δ 165.6, 149.8, 124.4, 117.7, 73.0, 22.3.

S2.7. Synthesis of 2,5-dipropoxyterephthalohydrazide

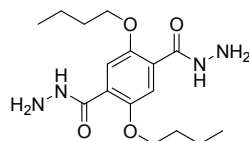


According to the reported method^{S1} by using diethyl 2,5-dipropoxyterephthalate as start material, the titled compound was collected with a yield of 79%.

^1H NMR (400 MHz, DMSO): (ppm) δ 9.21 (s, 2H), 7.38 (s, 2H), 4.58 (d, $J = 4.2$ Hz, 4H), 4.02 (t, $J = 6.5$ Hz, 4H), 1.83 – 1.68 (m, 4H), 0.98 (t, $J = 7.4$ Hz, 6H).

^{13}C NMR (100 MHz, DMSO): (ppm) δ 164.3, 150.2, 125.5, 115.2, 71.1, 22.4, 10.9.

S2.8. Synthesis of 2,5-dibutoxyterephthalohydrazide



According to the reported method^{S1} by using diethyl 2,5-dibutoxyterephthalate as start material, the titled compound was collected with a yield of 75%.

^1H NMR (400 MHz, DMSO) δ 9.20 (s, 2H), 7.38 (s, 2H), 4.57 (d, $J = 4.3$ Hz, 4H), 4.06 (t, $J = 6.5$ Hz, 4H), 1.79 – 1.65 (m, 4H), 1.50 – 1.33 (m, 4H), 0.94 (t, $J = 7.4$ Hz, 6H).

^{13}C NMR (100 MHz, DMSO): (ppm) δ 164.3, 150.2, 125.5, 115.5, 69.3, 31.1, 19.1, 14.2.

S2.9. Synthesis of COF-X15, COF-X20 and COF-X21

The procedures of synthesize these three COFs were the same as the synthesis of COF-42, the only differences are the starting materials. Therefore, start with 2,5-diisopropoxyterephthalohydrazide, 2,5-dipropoxyterephthalohydrazide and 2,5-dibutoxyterephthalohydrazide, COF-X15, COF-X20 and COF-X21 were synthesized respectively. The synthesized COFs were dried at 100 °C in a vacuum oven overnight before use.

S3. Compatibility and crosslinking density characterization

The crosslinking density of the membrane selective layer was detected using a nuclear magnetic resonance (NMR) crosslinking density spectrometer (MRCDS, VTMR20-010V-T, Shanghai Niumag Corporation, China) at a magnetic field strength of 0.5 Tesla under 35 °C, corresponding to 21.306MHz proton resonance frequency and 10 mm coil diameter. The circular samples with about 8 mm thickness and 6~9 mm diameter were put into the glass tubes and placed into the magnet filed of the spectrometer. The measurements were carried out at a temperature of 80 °C. The crosslinking

density software and inversion software were adopted to analyze the tested data. The detailed analysis model and calculation process were shown as follows:

In the NMR Analysis System Software, the XLD model is based on the NMR transverse relaxation which is caused by the dipole-dipole interaction of the intra- and inter-molecular hydrogen proton. The internal composition of the polymer is divided into two kinds of crosslinked chains and the dangling chains. The XLD test model mathematical formula is:^{S2,S3}

$$M(t) = A * \exp\left(-\frac{t}{T_{21}} - 0.5 * qMr1t^2\right) + B * \exp\left(-\frac{t}{T_{21}}\right) + C * \exp\left(-\frac{t}{T_{22}}\right) + A_0 \quad (1)$$

where $M(t)$ represents the magnetization at time t ; A , B and C represent the fractional contributions of the inter-crosslink chains (%), the dangling chains (%), and the sol signal (%), respectively; T_{21} and T_{22} are the relaxation times of inter-crosslink part and dangling part, and sol signal relaxation time, respectively; q is the anisotropy parameter of the inter-cross-linked chains; $Mr1$ is the residual dipolar coupling of the rigid lattice. The CPMG (Carr-Purcell-Meiboom-Gill) sequence was used to measure relaxation time T_{21} of inter-crosslink part and dangling part, and relaxation time T_{22} of sol signal. The following parameters were adopted: P90(us)=4, P180(us)=9, TD=40826, SW(KHz)=200, RFD(us)=200, TW(ms)=3000, RG1=20, RG2=3, NS=16, DL1(us)=0.196, NECH=8000.

The crosslinking density V_c was calculated as follows:

$$V_c = \frac{A * \rho}{M_c} \quad (2)$$

$$M_c = \frac{3cM_{ru}}{5N\sqrt{q}} \quad (3)$$

where ρ is the mass density (g/cm^3); M_c is the molecular mass of inter-cross-linked chains; c is the number of backbone bonds in a Kuhn segment;^{S4} M_{ru} is the molar mass of repeating units per number of backbone bonds (g/mol); N is number of back bone bonds in one unit.

Therefore, the cross linking density can be further simplified to the follow formula:

$$V_c = \frac{5\rho N\sqrt{q}}{3c_{\infty}M_{ru}} \quad (4)$$

The $qMrl$ value can be obtained according to the XLD model. As the parameters could be determined and then calculated, the crosslinking density (V_c) of the samples was ultimately obtained by the software.

S4. Simulation method

S4.1. Membrane model construction

Fig. S21a illustrates the initial structure of PDMS. Same as Ghoufi and Szymczyk's work^{S5}, a pre-PDMS membrane was generated by packing 110 PDMS chains into a simulation box (see **Fig. S21b**). The target packing density was 1.1 g cm^{-3} , higher than 1.083 g cm^{-3} as available in the literature^{S6}. A total of 9 pre-PDMS membrane configurations were further packed orderly into a simulation box along the xy-plane. The output coordinate file was used as the initial configuration for a 20ns NVT MD simulation ($T=300 \text{ K}$). The neat PDMS membrane was generated as shown in **Fig. S21c**. **Fig. S21d** illustrates the crystal structure of COF-42 constructed on the basis of experimental crystallographic data^{S7}. The COF-42 and 8 pre-PDMS membrane configurations was packed to generate the COF-42–PDMS membrane. The COF-42 was frozen in center of COF-42–PDMS membrane. After the 20ns NVT MD simulation ($T=300 \text{ K}$), the COF-42–PDMS membrane was generated (see **Fig. S21e**). Here, the topology of PDMS with 20 unit and COF-42 was generated using the PRODRG^{S8} web server. The MD simulation was conducted using GROMACS software v.5.1.7^{S9} and the GROMOS 53a6 force field.

S4.2. Simulation details

As shown in **Fig. S22a**, the dimensions of simulation box was set to be $192 \times 192 \times 600 \text{ \AA}^3$. A 420 \AA vacuum layer was added above the membrane and the thickness of our membrane is 100 \AA . To simulate 5 wt% butanol/water mixture, 14248 Tip3p water molecules and 160 butanol molecules were randomly placed on the feed side, with a thickness of 80 \AA . To study permeability and separation selectivity of water and butanol molecules, as seen the red arrow in **Fig. S22**, we put a biased 10Mpa pressure to the system by applying an external force to water and butanol molecules. The method of

applying pressure can be found in our previous work^{S10}. To keep the integrity of membrane, the geometry center of PDMS chain was fixed in the z direction. All atoms in COF-42 were frozen during simulations.

MD simulations were performed with the GROMACS software v.5.1.7^{S9} and the GROMOS 53a6 force field. The topology of butanol molecules were generated by ATB^{S11}. Two-dimensional periodic boundary condition (PBC) was used in xy directions. The particle mesh Ewald (PME) method^{S12} was employed to calculate the long-range electrostatic interaction with a cutoff of 13.0 Å. To calculate the long-range electrostatic interaction in the 2D-PBC simulation cell, the ewald-geometry option in gromacs mdp file was set to be 3dc. For each simulation, after energy minimization the system, 8ns simulation was carried out in NVT ensemble, temperature of system were kept at 353.15 K with Nosé-Hoover method.

S5. Supplementary Figures (Fig. S1 to Fig. S31)

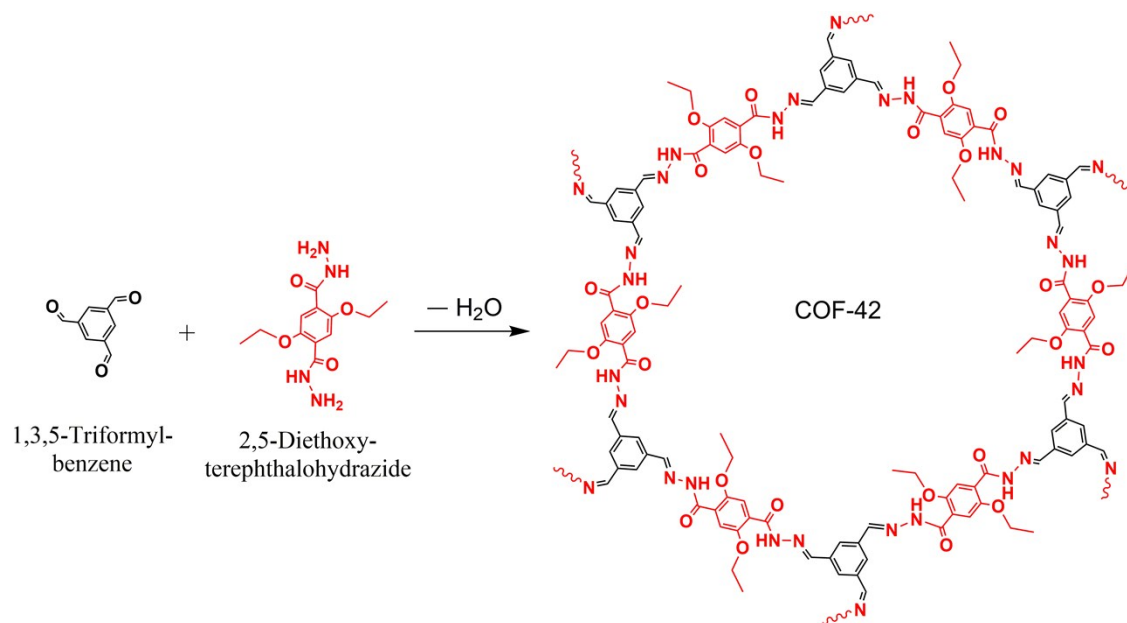


Fig. S1 Synthesis of COF-42 and its chemical structure.

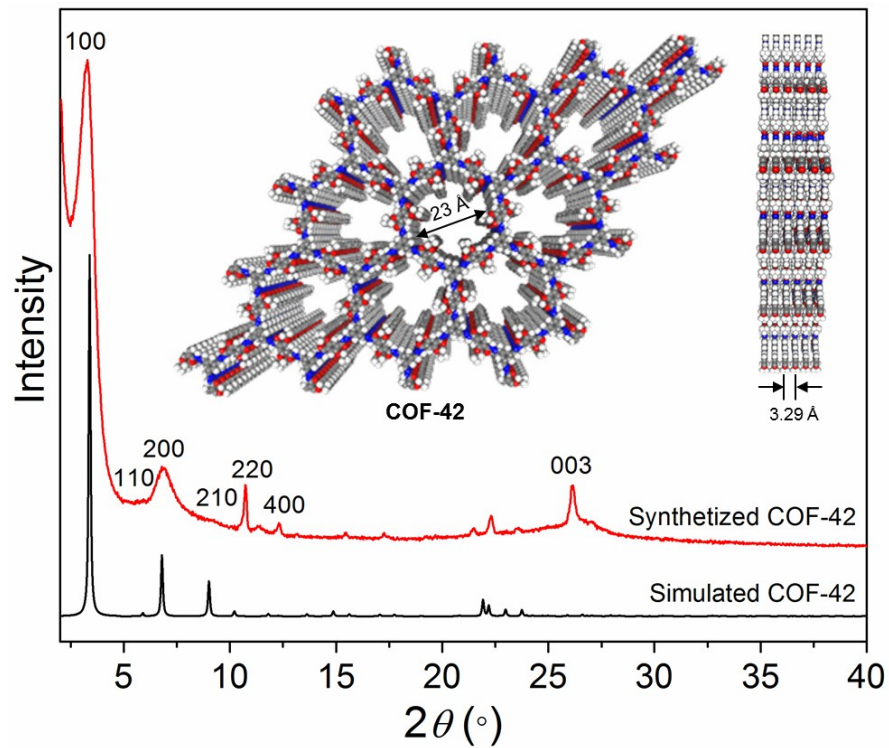


Fig. S2 Experimental and simulated PXRD patterns of COF-42 in eclipsed mode. (Inset images show crystal structures viewed through [001] (left) and [100] (right) directions). The simulated patterns were made by materials studio 8.0.

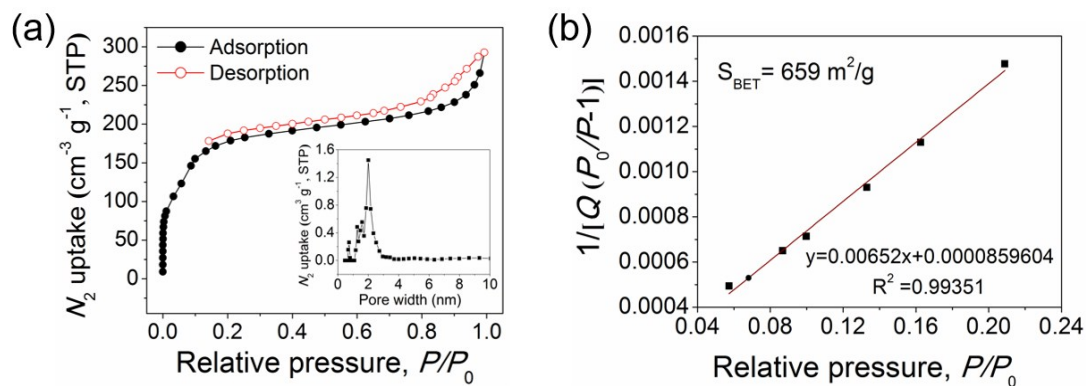


Fig. S3 (a) N_2 adsorption and desorption isotherms attached pore size distribution of the synthesized COF-42. (b) BET plot of COF-42 from N_2 adsorption data.

The N_2 adsorption measurement of COF-42, including type-IV profile and pore size distribution curve, is in overall agreement with data for COF-42 reported elsewhere^{S1}. The mesoporous volume is about $0.29 \text{ cm}^3 \text{g}^{-1}$, and the BET surface areas are $659 \text{ m}^2 \text{g}^{-1}$, respectively. The BET surface area is very close to that of reported COF-42 samples (BET surface area: $710 \text{ m}^2 \text{g}^{-1}$, mesoporous volume: $0.31 \text{ cm}^3 \text{g}^{-1}$)^{S1}.

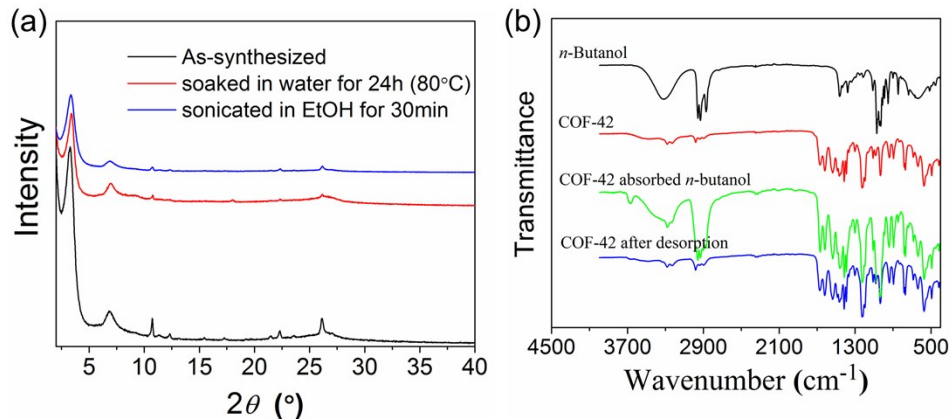


Fig. S4 Stability characterization of the synthesized COF-42. (a) PXRD patterns for the original, and the soaked COF-42. (b) ATR-FTIR spectra of the *n*-butanol, original COF-42, and the COF-42 after *n*-butanol adsorption and desorption.

The stability of COF-42 was investigated by soaking the powders in water and ethanol respectively, and the corresponding PXRD patterns were measured. As shown in **Fig. S4a**, the good crystallinity of COF-42 samples was retained after processing, although there were some slight differences of the peak strength ratio. Furthermore, the attenuated total reflectance-fourier transform infrared spectra (ATR-FTIR) suggested the butanol adsorption in COF-42 is a physical adsorption, and the butanol could be desorpted completely because there is no apparent shifts and redundant peaks in the bands for the COF-42 adsorbed *n*-butanol and no *n*-butanol peaks present in the COF-42 after desorption (**Fig. S4b**). These results indicate the excellent stability of COF-42 in liquid under harsh conditions.

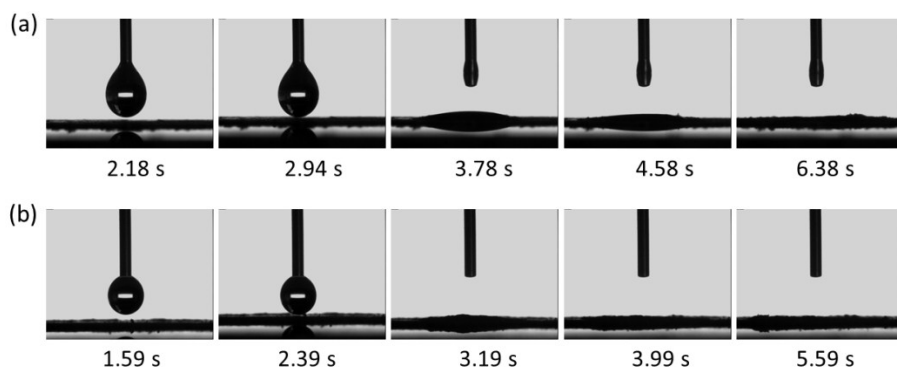


Fig. S5 (a) *n*-butanol and (b) water contact angle changes of the as-synthesized COF-42 powders versus testing time.

As shown in the **Fig. S5**, both *n*-butanol and water drop profiles were fast spread out when contacting the powder surfaces and the corresponding contact angles decreased to zero only within 4 s. This suggests the porous COF-42 framework is amphipathic (hydrophilic and alcoholphilic). We think the hydrophilicity may be due to the existence of carbonyl groups (C=O), and the alcoholphilicity can be attributed to the hydrazone linked skeleton and the abundant vinyl groups inside the pore walls. This feature is also conducive to the significant improvement of permeation flux by the simultaneous adsorption of *n*-butanol and water in membrane.

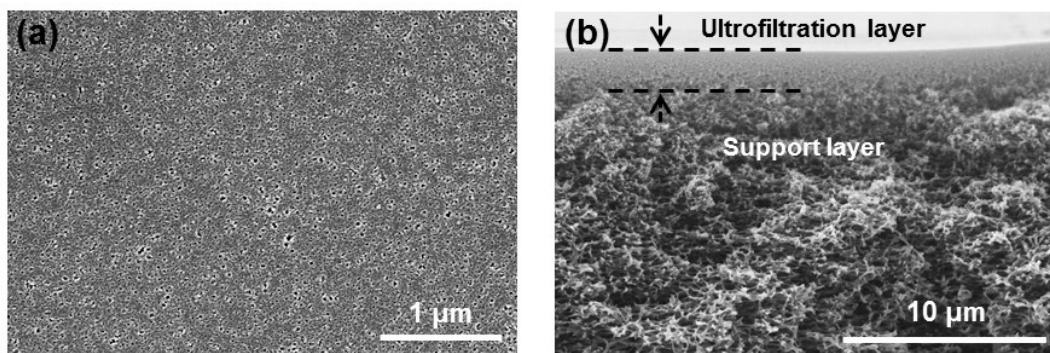


Fig. S6 (a) Surface and (b) cross-sectional SEM images of the porous PSf supporting membrane.

As shown in **Fig. S6a**, the membrane surface was porous and the pore size is about 30 nm in diameter. From **Fig. S6b**, there is a 2 μm-thick ultrafiltration layer near the top surface of the membrane cross-section.

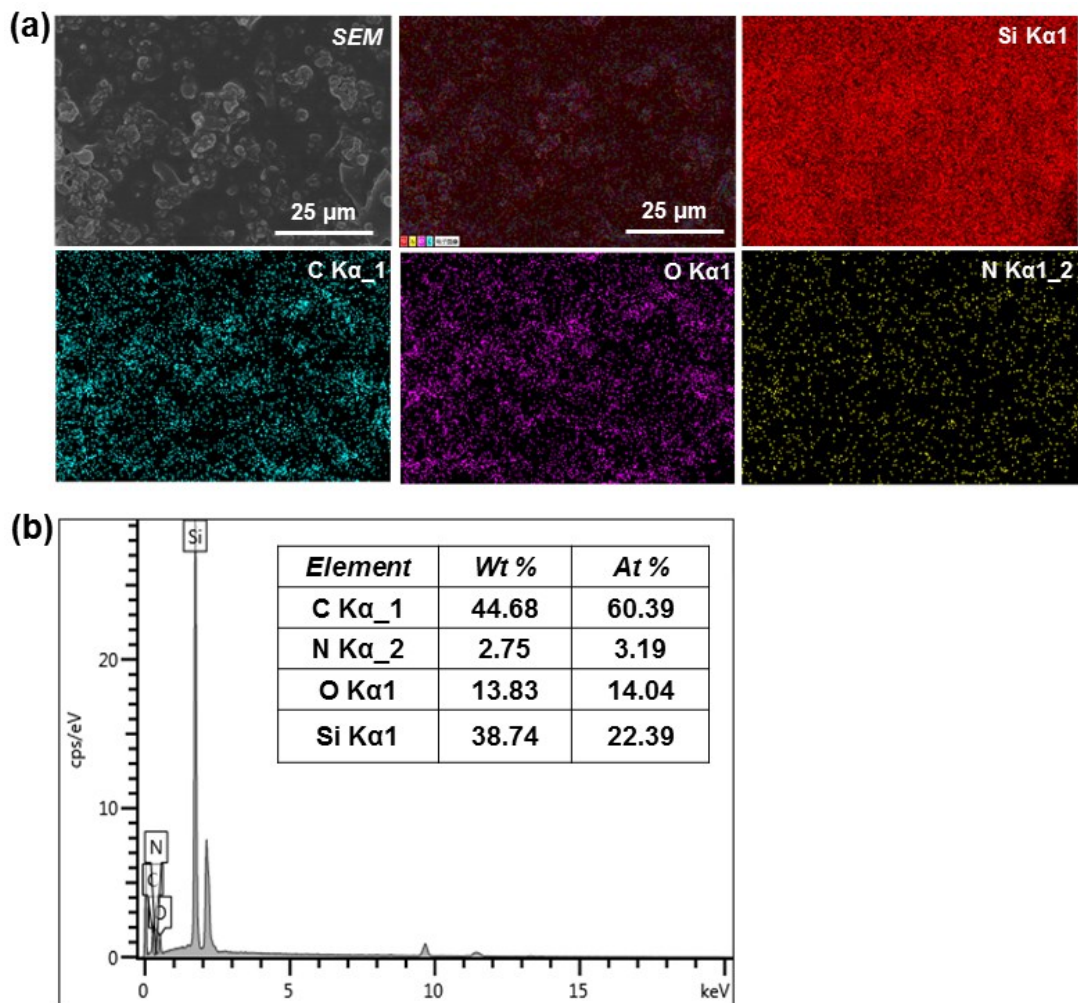


Fig. S7 (a) SEM image of the top view and corresponding EDS mapping of the COF-42-PDMS membrane (1 wt% of COF-42 loading). (b) EDS spectrum and the inserted table of elemental contents.

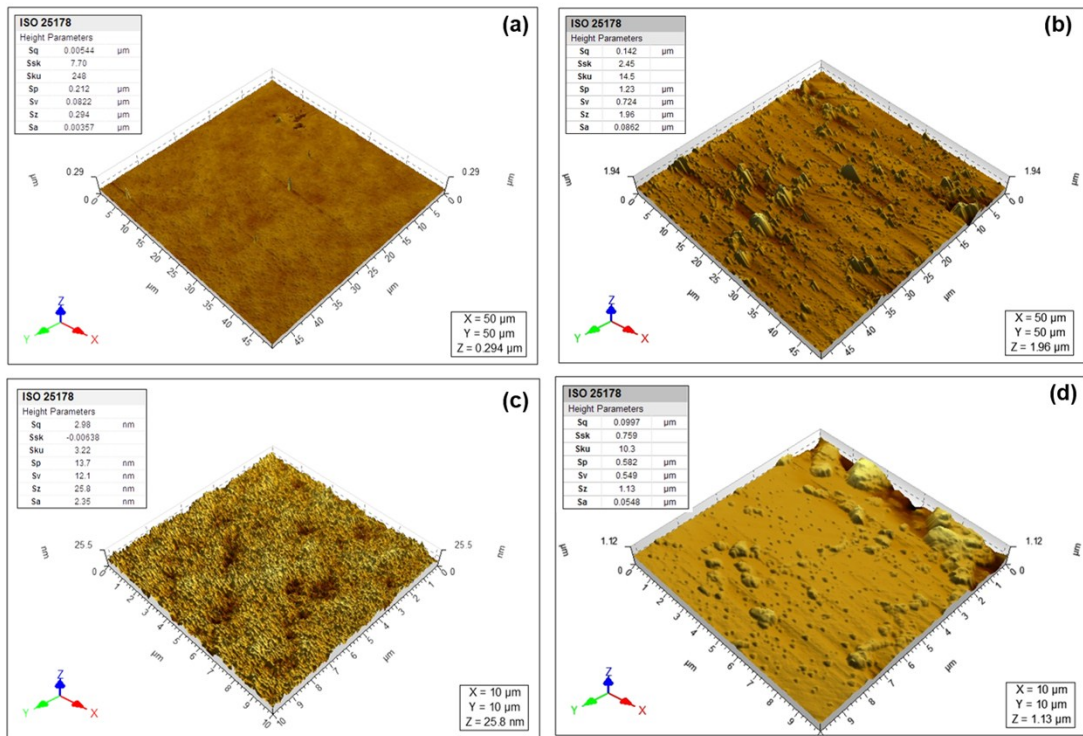


Fig. S8 3D surface AFM images of porous PSf membrane (a) 50 $\mu\text{m} \times 50 \mu\text{m}$, (c) 10 $\mu\text{m} \times 10 \mu\text{m}$, and COF-42-PDMS membrane (b) 50 $\mu\text{m} \times 50 \mu\text{m}$, (d) 10 $\mu\text{m} \times 10 \mu\text{m}$ (Inserted images in top-left corner show the surface root mean square roughness (Sq)).

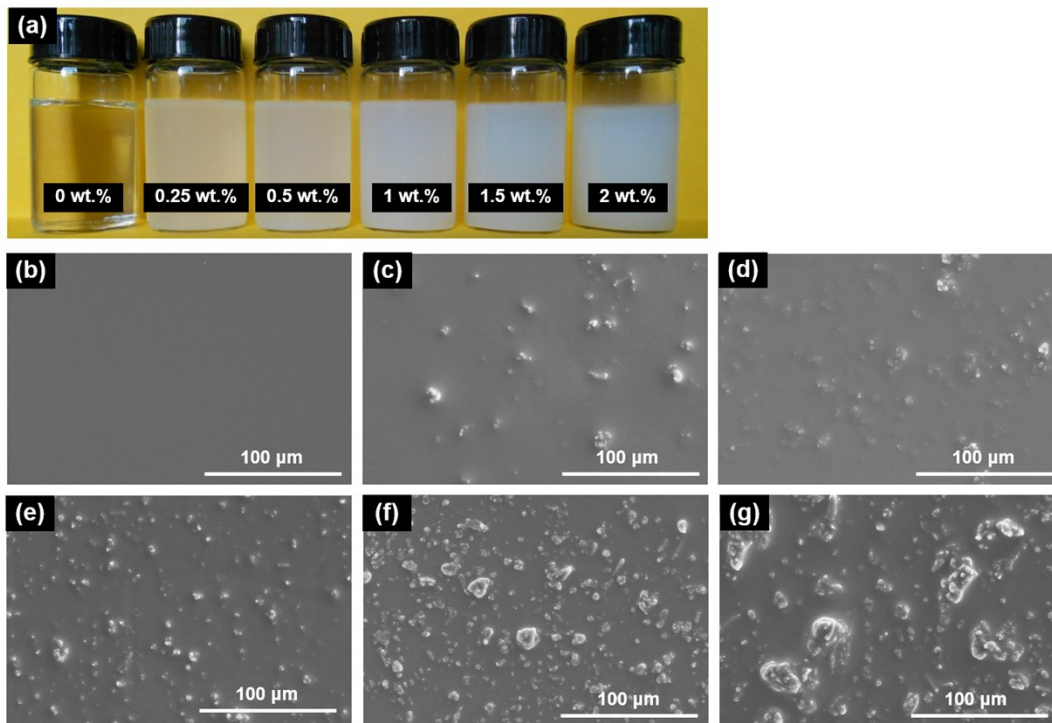


Fig. S9 (a) Digital photos of PDMS/COF-42 solutions with different COF-42 loading. Surface SEM images of COF-42-PDMS membrane with different COF-42 loadings, (b) 0 wt% (PDMS membrane), (c) 0.25 wt%, (d) 0.5 wt%, (e) 1 wt%, (f) 1.5 wt% and (g) 2 wt%.

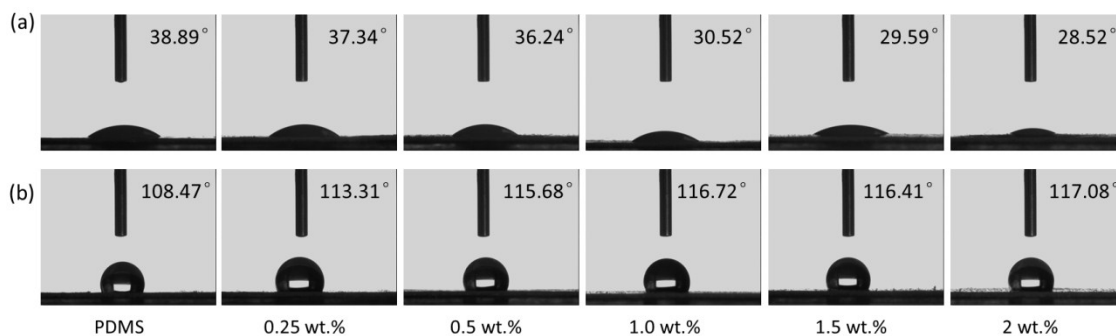


Fig. S10 (a) *n*-butanol and (b) water drop profiles combined corresponding contact angle values (right-upper corner) on the original PDMS membrane and COF-42–PDMS membrane with different COF loading.

It can be observed that the *n*-butanol contact angle decreased and the water contact angle increased with the increase of COF-42 loading in membrane. But the contact angle values varied only in a small range of about 10°, which suggests that the presence of the COF did not significantly change the wettability of membrane surface. The main reason is due to the amphipathicity of COFs and the coverage of PDMS on the COF surface.

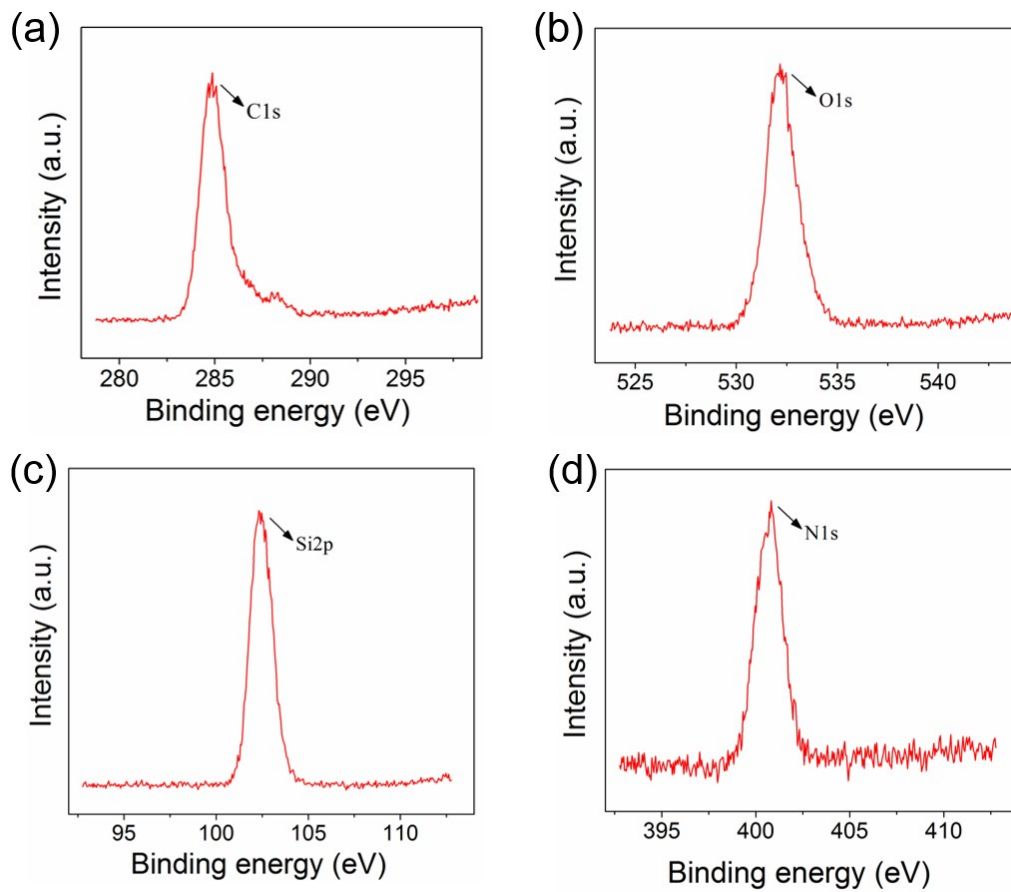


Fig. S11 (a) Enlarged XPS of Figure 2f for C1s site; (b) the enlarged XPS for O1s site; (c) the enlarged XPS for Si2p site; (d) the enlarged XPS for N1s site.

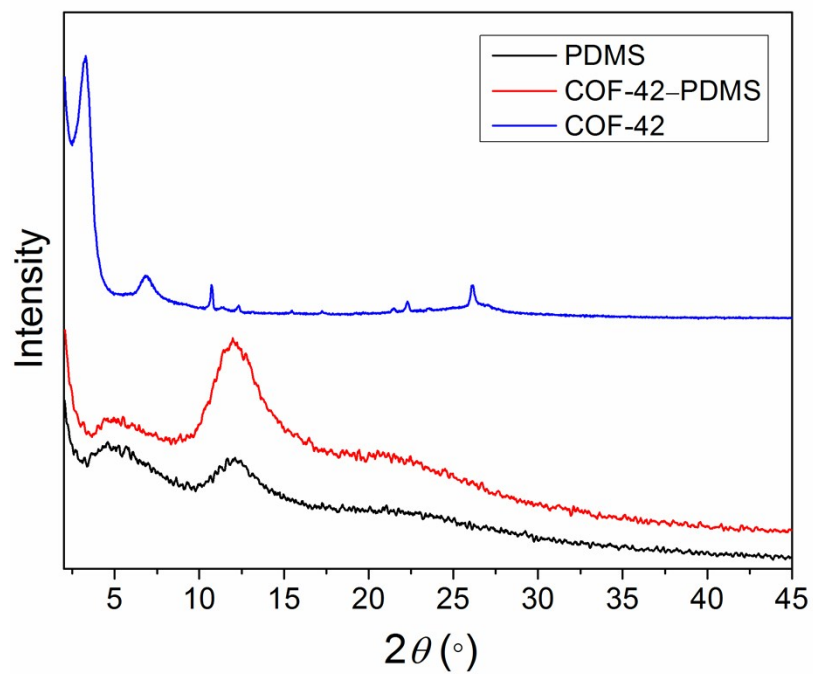


Fig. S12 XRD patterns of the synthesized COF-42, crosslinked PDMS layer and COF-42-PDMS layer (1 wt% COF-42 loading).

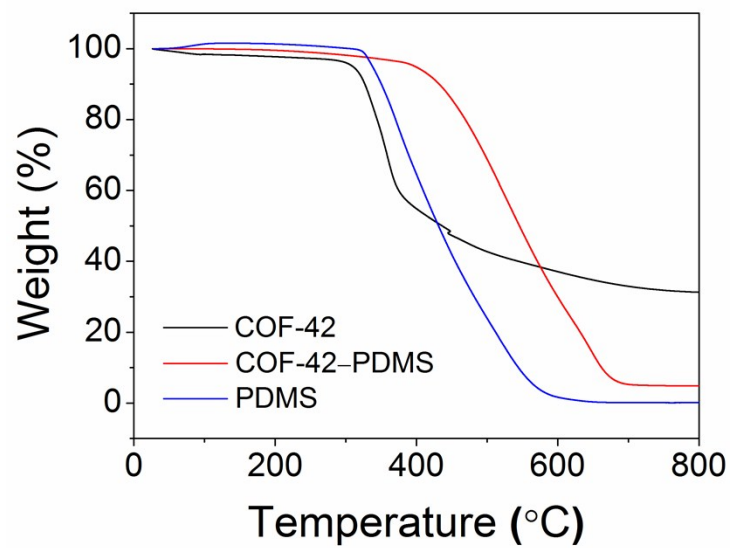


Fig. S13 TGA curves of COF-42, pure PDMS membrane, and COF-42-PDMS membrane (1wt% COF-42 loading).

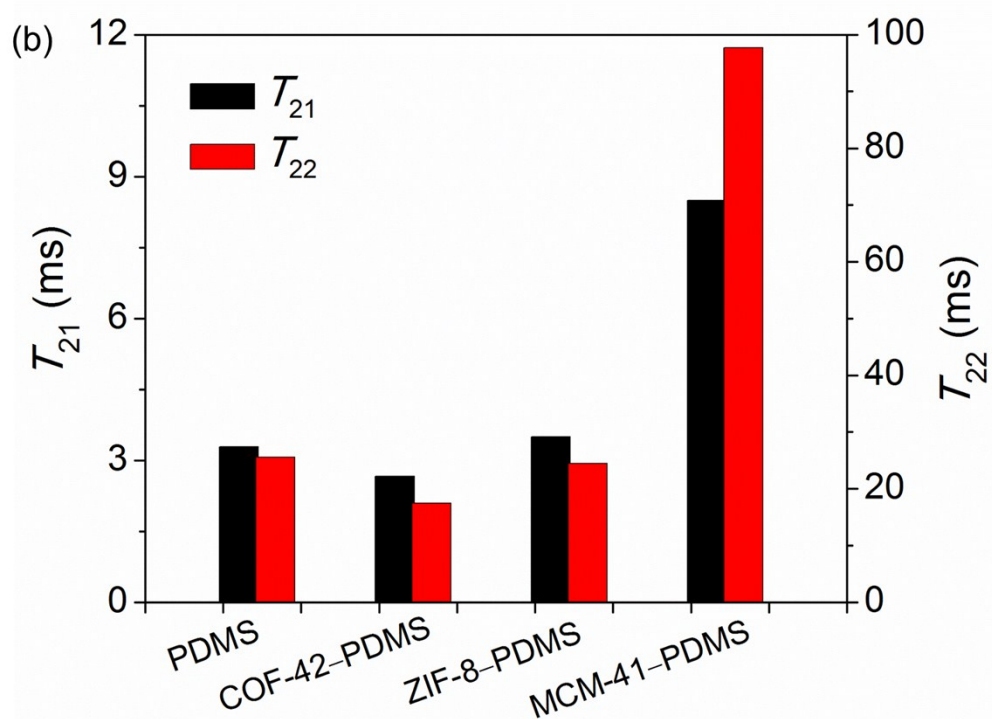
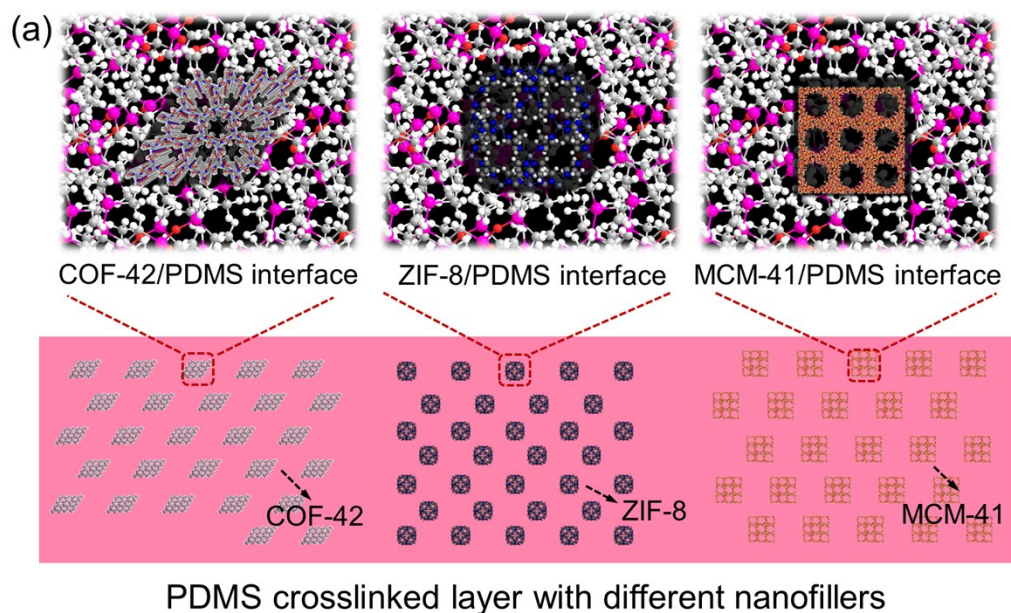


Fig. S14 (a) Schematic representation of interfaces in COF-42, ZIF-8 and MCM-41 incorporated PDMS crosslinked layers. (b) Interfacial relaxation time (T_{21}) and sol signal relaxation time (T_{22}) of PDMS crosslinked layer, and corresponding COF-42-PDMS, ZIF-8-PDMS and MCM-41-PDMS selective layers.

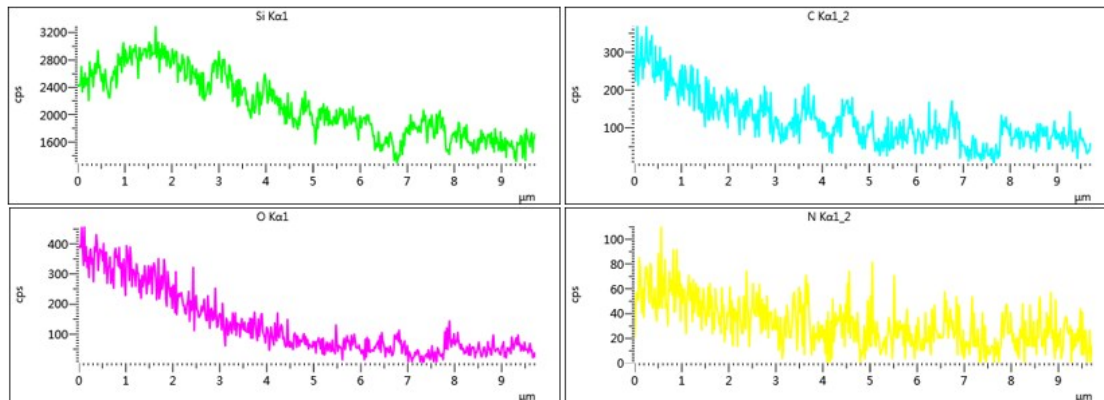


Fig. S15 Unfolded elemental EDS maps-linescan analysis across the cross-section of COF-42–PDMS membrane (starting from the membrane top surface of 0 μm).

In order to more accurately determine the thickness of COF-42–PDMS selective layer, we analyzed the changes in elemental composition through the cross-section near the top surface. As shown in elemental maps-linescan (**Fig. S15**), the silicon element was accumulated mainly before a depth of 6 μm and then its content decreased gradually, while the sulfur content increased obviously after reaching a depth of 3 μm . Since the PSf membrane did not contain silicon and PDMS did not contain sulfur, the silicon element came from the selective layer and the sulfur came from the PSf supporting membrane. These results suggested that the formed COF-42–PDMS layer may have penetrated into the pores of the PSf supporting membrane, and the layer thickness was about 3 μm . It should be noted that the observed nitrogen signals always remained low, mainly due to the relatively small amounts of COF-42 in the selective layer.

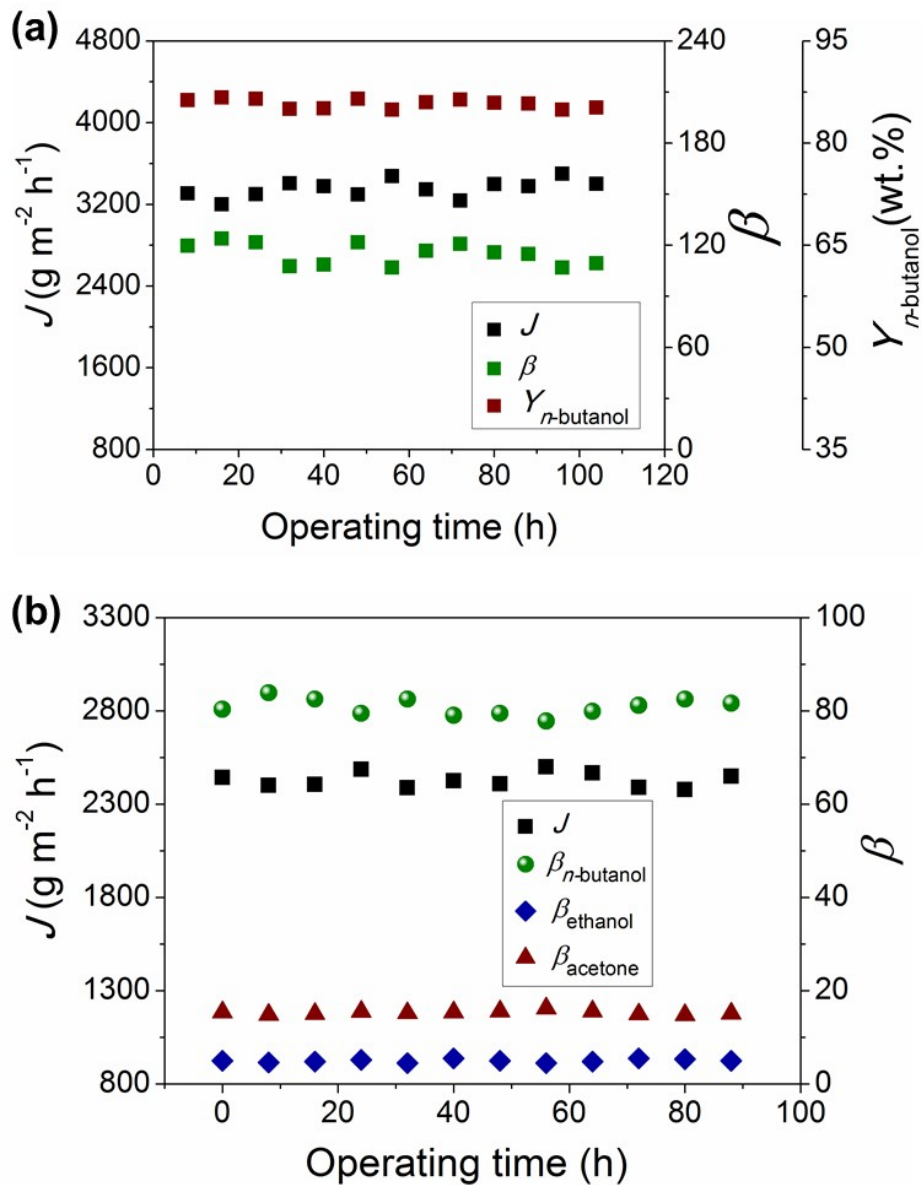


Fig. S16 (a) Stability test of COF-42-PDMS membrane through a continuous pervaporation process for 5.0 wt.% *n*-butanol aqueous solution at 80 °C. (b) Overall performance test of COF-42-PDMS membrane by using model acetone-butanol-ethanol (ABE) fermentation froth (3.6 wt% *n*-butanol, 1.8 wt% acetone and 0.6 wt% ethanol in aqueous solution, 80 °C) as the feed.

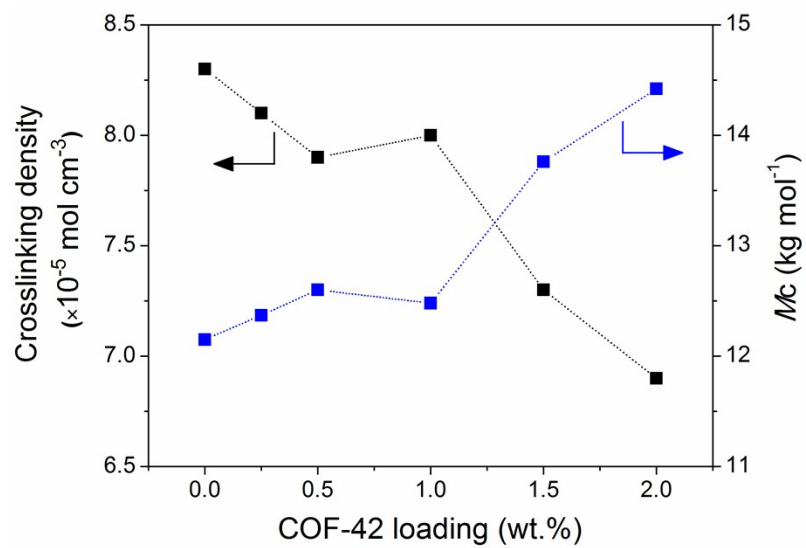


Fig. S17 Crosslinking density and M_c of the COF-42–PDMS selective layer with different COF-42 loading.

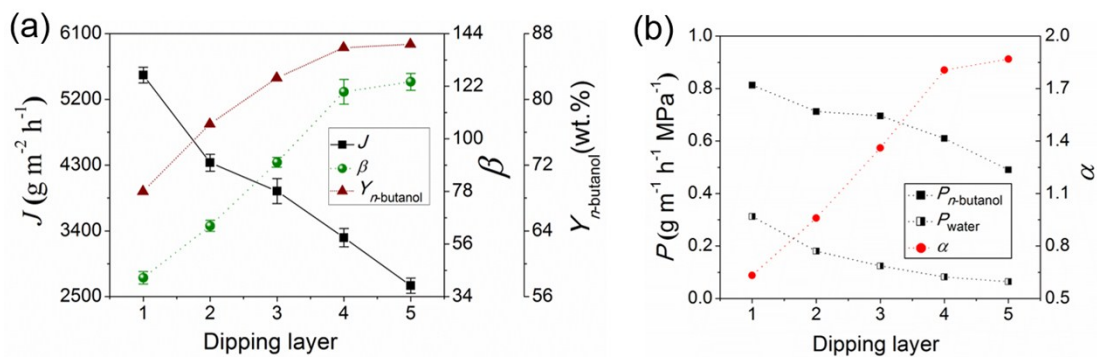


Fig. S18 Effect of dipping layer on the pervaporation performance of the COF-42-PDMS membrane (1wt% COF-42 loading), (a) flux, separation factor and permeate concentration; (b) permeability and selectivity. Feed solution, 5 wt.% *n*-butanol aqueous solution at 80 °C. Error estimates were varied from 2.0% to 4.3% for the flux and from 2.2% to 6.3% for the separation factor.

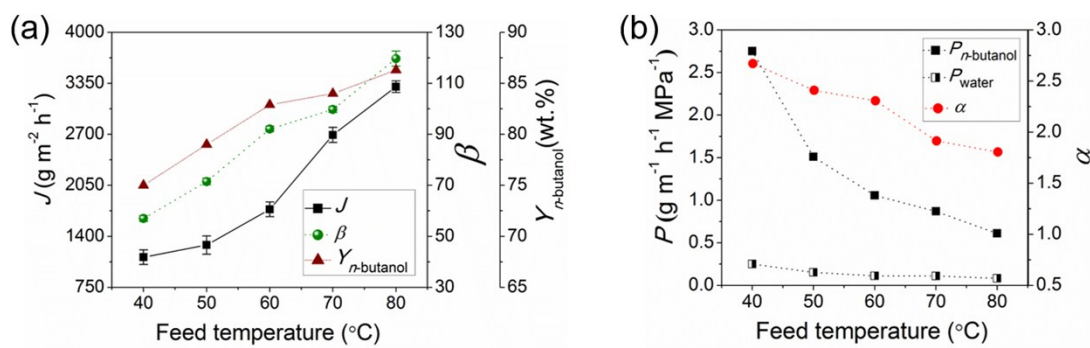


Fig. S19 Effect of feed temperature on the pervaporation performance of the COF-42-PDMS membrane, (a) flux and separation factor, (b) permeability and selectivity. Error estimates were varied from 2.2% to 8.2% for the flux and from 1.2% to 5.6% for the separation factor.

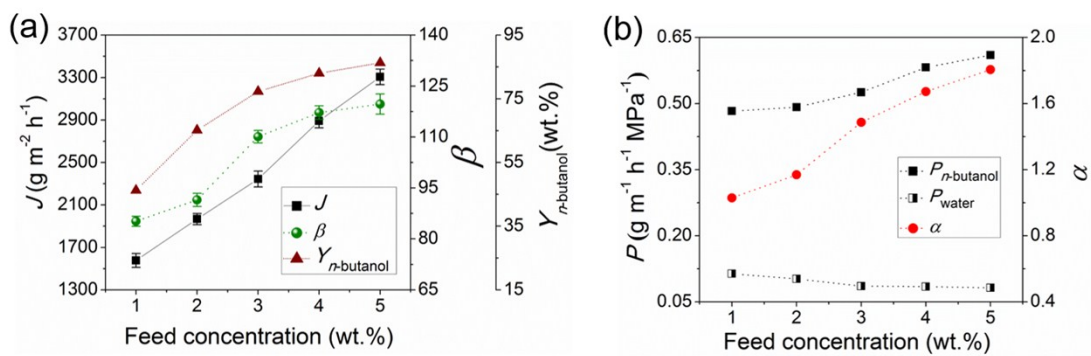


Fig. S20 Effect of feed concentration on the pervaporation performance of the COF-42-PDMS membrane, (c) flux and separation factor, (d) permeability and selectivity; Error estimates were varied from 3.8% to 7.1% for the flux and from 1.7% to 4.2% for the separation factor.

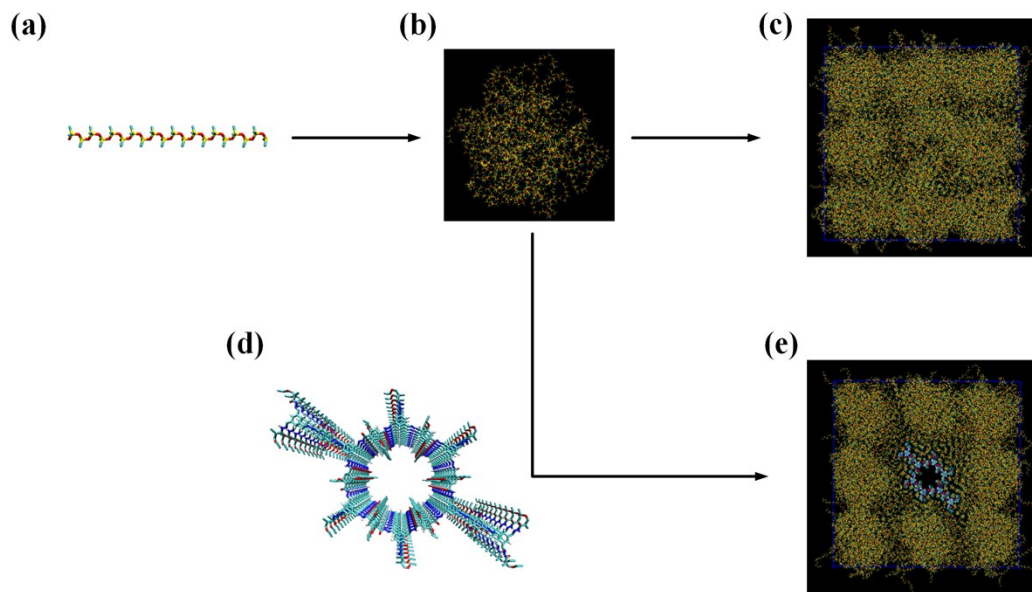


Fig. S21 Schematic illustration showing the construction of PDMS and COF-42-PDMS membrane model. (a) The initial structure of PDMS with 20 unit, (b) pre-PDMS membrane, (c) neat PDMS membrane, (d) COF-42 unit cell, (e) COF-42-PDMS membrane (some hydrogen atoms are not shown). Color code: N, blue; H, white; O, red; C, cyan; and Si, yellow.

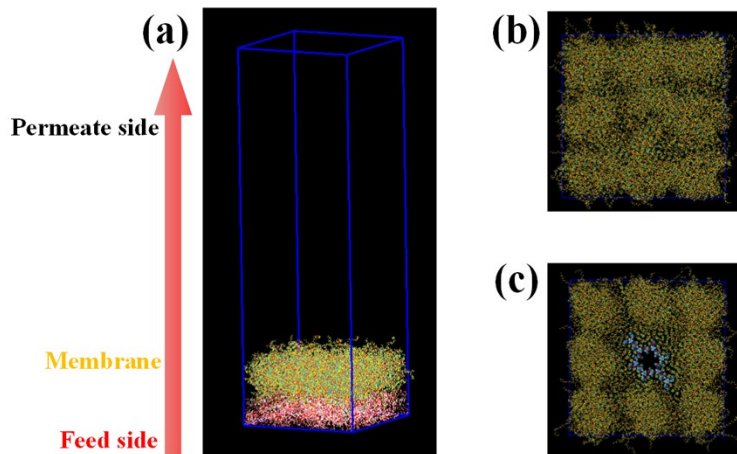


Fig. S22 (a) Snapshot of the initial configuration for simulation of water/butanol permeation through the membrane. (b) Top view of PDMS membrane, (c) Top view of COF-42–PDMS membrane. The showed color code is the same as **Fig. S22**

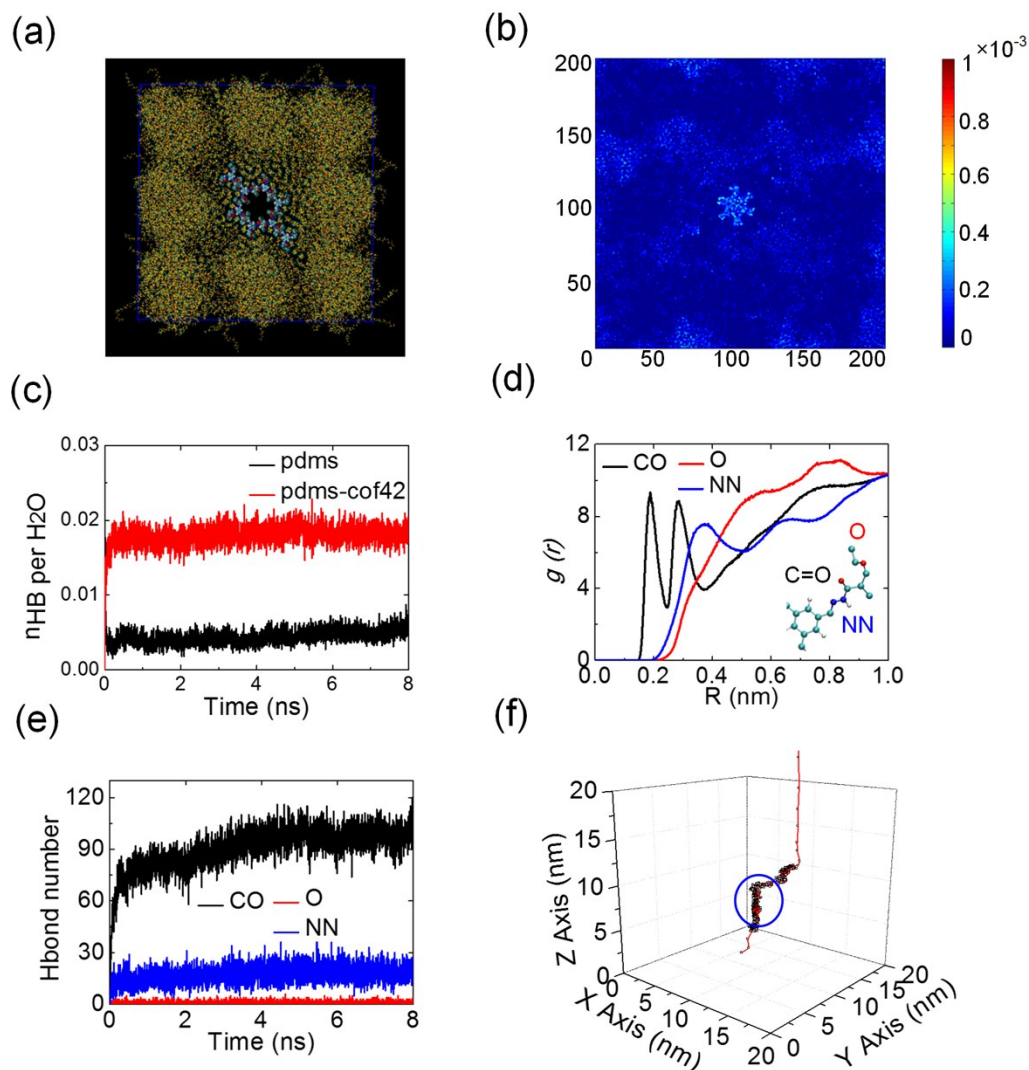


Fig. S23 MD simulations. (a) Top view of simulated COF-42-PDMS membrane. (b) Simulated density distribution of water molecules in the COF-42-PDMS membrane in x-y plane. (c) Number of hydrogen bonds (HBs) per water molecule formed between water and membrane. (d) The RDFs of water molecules around different groups in COF-42, (e) Number of HBs formed between water and different groups in COF-42. (f) Trajectories of an *n*-butanol molecule passing through COF-42 (within the blue circle).

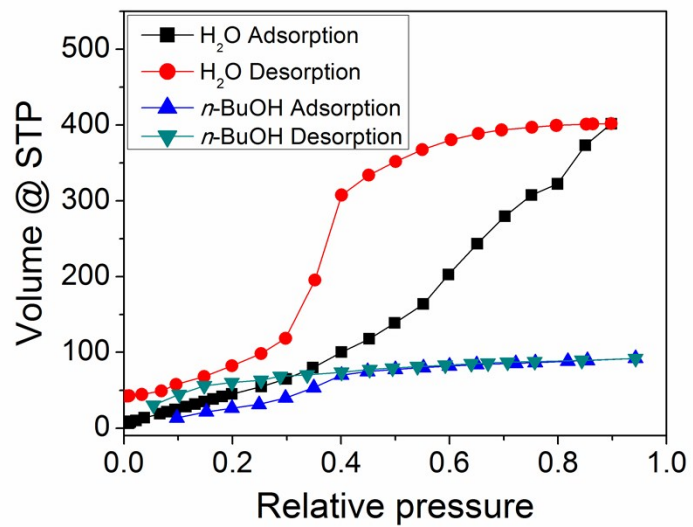


Fig. S24 Adsorption-desorption curve of COF-42 materials to *n*-butanol and water molecules.

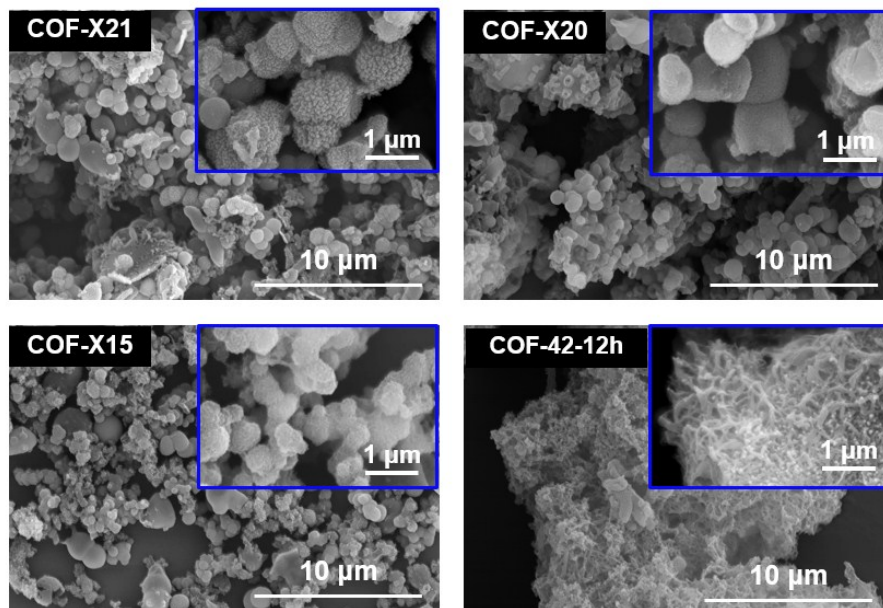


Fig. S25 SEM images with inserted magnification (top-right corner) of the synthesized COF-X21, COF-X20, COF-X15 and COF-42-12h.

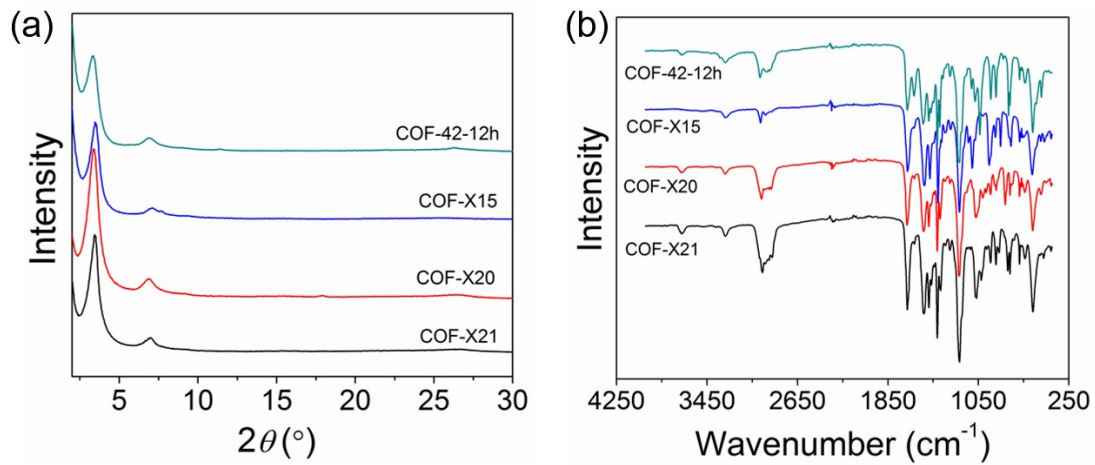


Fig. S26 (a) PXRD patterns and (b) ATR-FTIR spectra of the synthesized different COF materials.

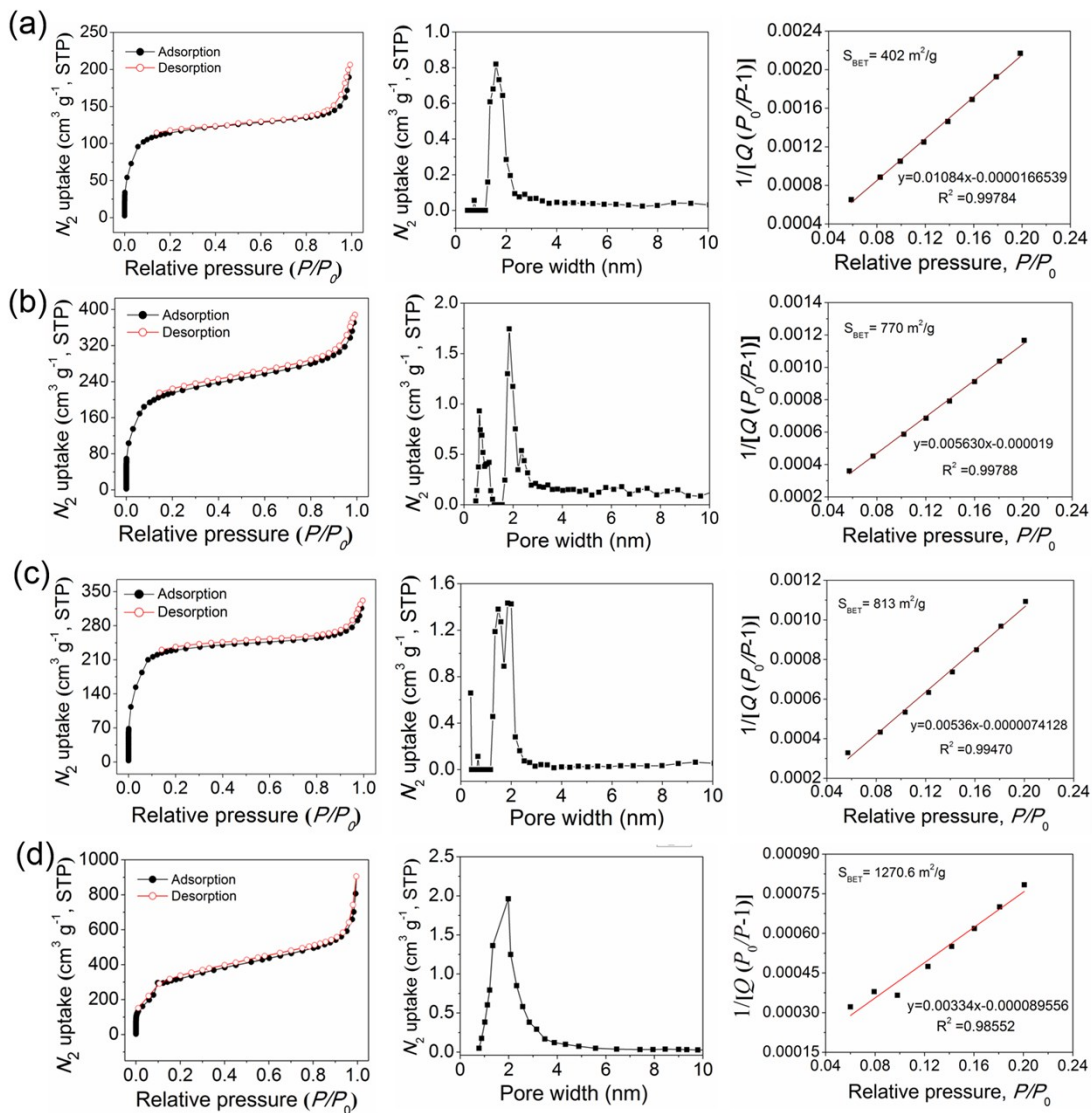


Fig. S27 N_2 adsorption and desorption isotherms (left), pore size distribution (middle) and BET plot (right) of synthesized (a) COF-X21, (b) COF-X20, (c) COF-X15 and (d) COF-42-12h.

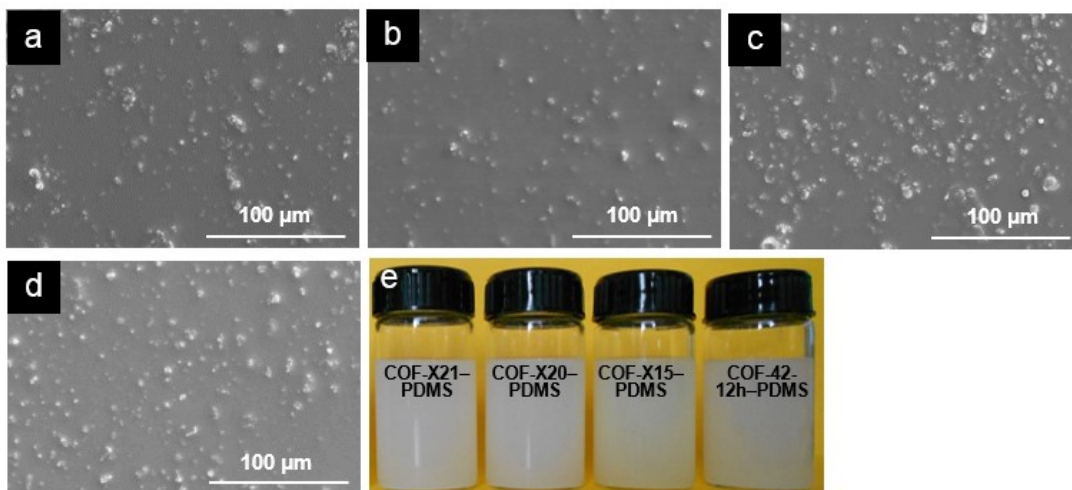


Fig. S28 Surface SEM images of corresponding COF-based membranes with 1 wt% COF loading, (a) COF-X21-PDMS membrane, (b) COF-X20-PDMS membrane, (c) COF-X15-PDMS membrane and (d) COF-42-12h-PDMS membrane. (e) Digital photo of corresponding PDMS/COF solution.

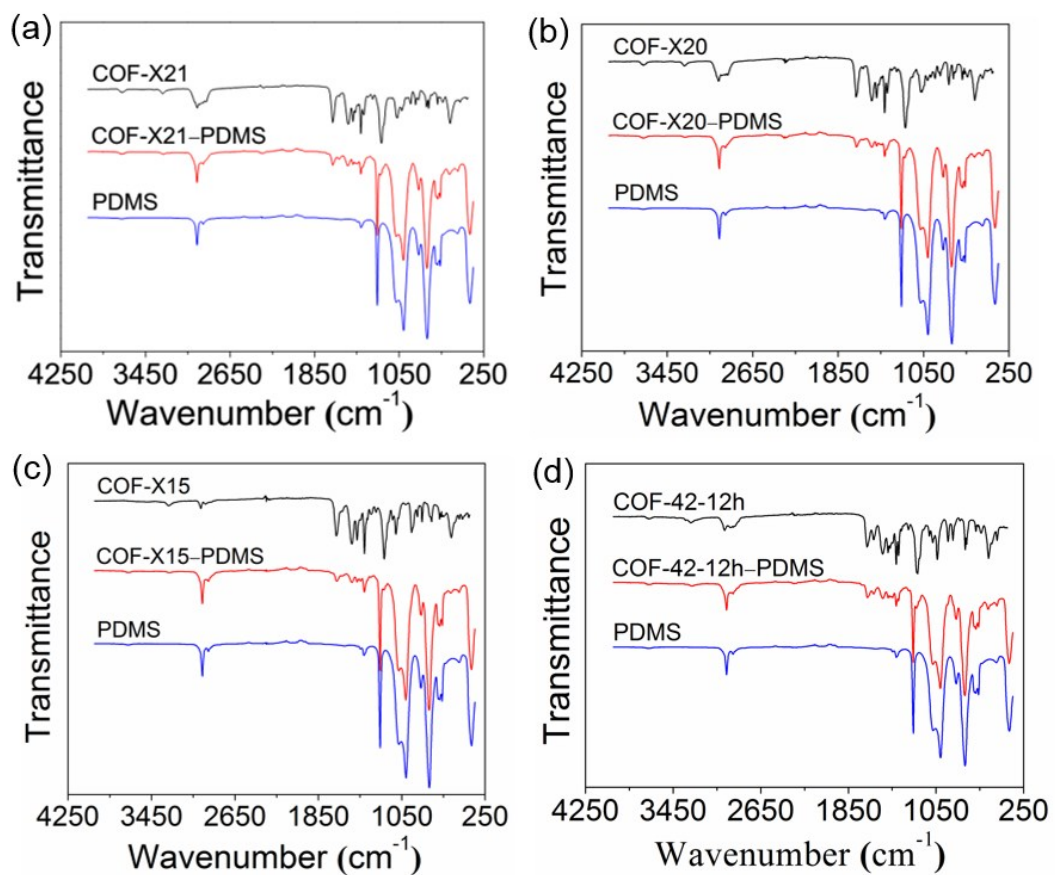


Fig. S29 ATR-FTIR spectra analysis of different COF-based membranes.

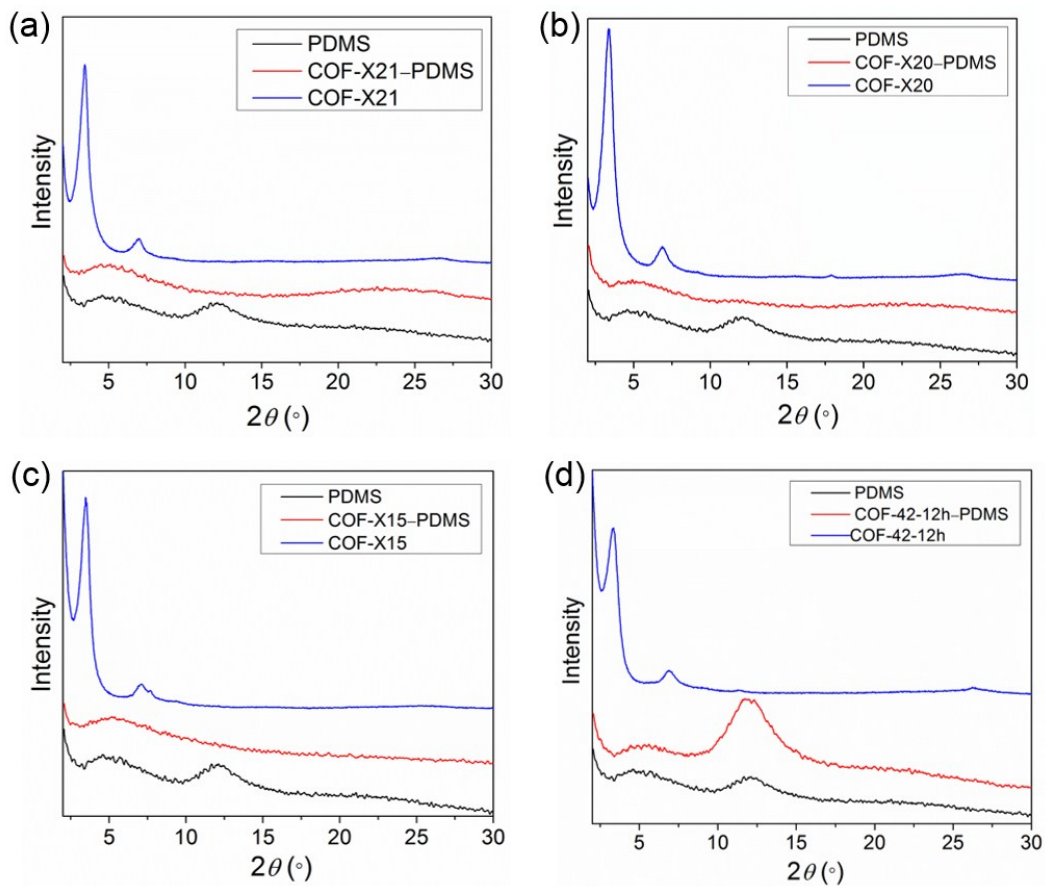


Fig. S30 XRD patterns of corresponding COF-based membrane selective layers, (a) COF-X21-PDMS membrane, (b) COF-X20-PDMS membrane, (c) COF-X15-PDMS membrane and (d) COF-42-12h-PDMS membrane.

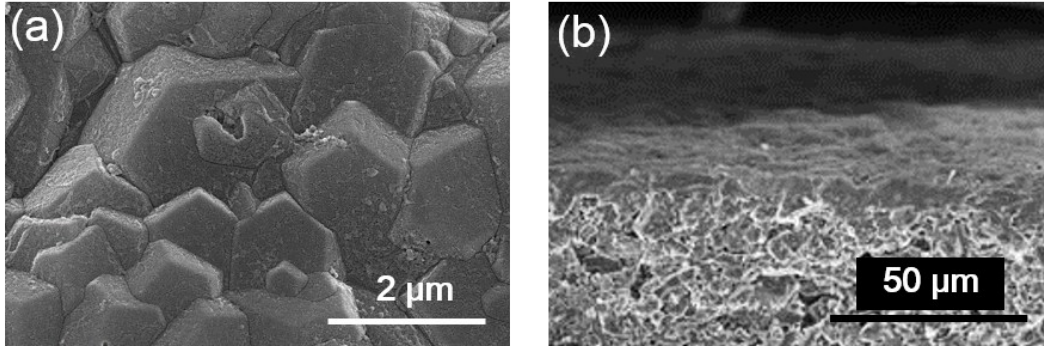


Fig. S31 (a) External Surface and (b) cross-sectional SEM images of the hydrophilic NaA tubular ceramic membrane (supplied by Beijing Hongzhi Jiahe Co., Ltd.).

S6. Supplementary Tables (Table S1 to Table S2)

Table S1 Simulated diffusion coefficient of water and *n*-butanol.

Material type	Diffusion Coefficient / $\times 10^{-5} \text{ nm}^2 \text{ s}^{-1}$	
	Water	<i>n</i> -butanol
PDMS	0.48 ± 0.11	0.11 ± 0.01
COF-42-PDMS	2.30 ± 0.14	5.36 ± 0.38
Hydrophobic "COF-42-PDMS" ^a	1.28 ± 0.30	0.11 ± 0.00

a: the atomic charges of COF-42-PDMS were tuned off

Table S2 Comparison of pervaporation performance for butanol/water mixture between various membranes.

Membrane type	Selective thickness (μm)	Feed conc. (wt.%)	Feed temp. ($^{\circ}\text{C}$)	Downstream pressure (kPa)	J ($\text{g m}^{-2} \text{h}^{-1}$)	β	Conc. in permeate (wt.%)	Ref.
PPhS/PDMS/PVDF	10	1 ^a	30	0.133	261.4	46.82	32.1 ^a	S13
CMX-GF-010-D	10	1 ^a	37	<0.3	330	39	28.3 ^a	S14
PERTHESE 500-1	125	1 ^a	37	<0.3	33	56	36.1 ^a	S14
PDMS/PE/Brass	65	1 ^a	37	<0.13	95	34	25.6 ^a	S15
PERVAP-2200	2	1 ^a	37	<1	330	10	9.2 ^a	S16
ZIF-71-PEBA	10-20	1 ^a	37	<0.4	520.2	18.8	16.0 ^a	S17
PDMS/ceramic	10	1 ^a	40	<0.4	457	26	20.8 ^a	S18
Silicalite/PDMS	15	1 ^a	40	0.07-0.4	134	92	48.2 ^a	S19
PERVAP-1070	210	1 ^a	40	0.2	90	36	26.7 ^a	S20
PDMS/hollow fiber	10	1 ^a	40	<0.4	1282	42.9	30.2 ^a	S21
POSS/PDMS	9	1 ^a	40	<0.4	745	40	28.8 ^a	S22
PDMS/PAN	4	1 ^a	42	0.1	1390	22	18.2 ^a	S23
Silicalite/PDMS	—	1 ^a	45	<0.67	250	32	24.4 ^a	S24
PTFE	40	1 ^a	50	—	805	10	9.2 ^a	S25
Silicate-1/PDMS	60	1 ^a	50	—	60	60	37.7 ^a	S26
PDMS/PEI	0.7	1 ^a	60	—	290	74	42.8 ^a	S27
Zn(BDC)(TED) _{0.5} /PEBA	10-20	1 ^a	60	<0.4	1300	20	16.8 ^a	S28
Silicone-silicalite-1	306	1 ^a	78	0.27-0.67	70	110	52.6 ^a	S29
ZIF-8-PDMS	0.8	1 ^a	80	<0.2	4846.2	81.6	45.2 ^a	S30
Silicalite-PDMS	0.3	1 ^b	80	—	7100	32	24.4 ^b	S31
ZIF-8-PMPS	2.5	1 ^b	80	—	6400	40.1	28.8 ^b	S32
PDMS ^c	30	1.5 ^a	55	0.2	670.2	43.1	39.6 ^a	S33
PTMSP	22	1.5 ^a	70	0.27	1030	70.0	51.6 ^a	S34
PTMSP/PDMSM	30	2 ^a	25	<0.266	120	128	72.3 ^a	S35
MCM-41-PEBA	30	2.5 ^a	35	—	500	25	39.1 ^a	S36
MFI	0.5	3 ^a	60	—	3600	10	23.6 ^a	S37
PET/PAN/PDMS	2.3	3.5 ^b	30	0.133	400	22	44.4 ^b	S38
PEBA	30	5 ^a	23	0.6	179	5.9	23.7 ^a	S39
PhTMS	30	5 ^a	30	<0.3	700	27	58.7 ^a	S40
PEBA-IL	5	5 ^a	37	—	560	23.2	55.0 ^a	S41
PDMS-ZIF-71	12	5 ^c	50	—	1500	30.2	61.4 ^c	S42
PDMS ^{CF3}	1	5 ^a	60	0.1	1292.8	27.3	59.0 ^a	S43
ZIF-8/PDMS	1.8	5 ^a	80	<0.2	2800.5	52.81	73.5 ^a	S44
PVDF	10	7.5 ^a	50	6.7	4126	6.4	34.2 ^a	S45
COF-42-PDMS	3	1 ^a	80	<0.2	1577.1	85.2	46.3 ^a	This work
		2 ^a	80	<0.2	1967	91.5	65.1 ^a	This work
		3 ^a	80	<0.2	3306.7	119.7	86.3 ^a	This work
		5 ^a	80	<0.2	3306.7	119.7	86.3 ^a	This work

^a*n*-Butanol aqueous solution; ^b*iso*-Butanol aqueous solution; ^c*sec*-Butanol aqueous solution.

PPhS: Polyphenylsiloxane; PhTMS: (glassy) Phenyltrimethoxysilane; PDMS: Poly(dimethyl siloxane); PVDF: Polyvinylidene fluoride; PE: Poly Ethylene; PEBA: Poly(ether-block-amide); POSS: Polyhedral oligomeric silsesquioxanes; PAN: Polyacrylonitrile; PTFE: Polytetrafluoroethylene; PEI: Polyetherimide; PMPS: Polymethylphenylsiloxane; PTMSP: Poly(1-trimethylsilyl-1-propyne); PDMSM: Poly(dimethylsilmethylene); PET: Polyester; IL: Ionic liquid; Zn(BDC)(TED)_{0.5}: (BDC = benzenedicarboxylate, TED = triethylenediamine).

Reference

- S1. F. J. Uribe-Romo, C. J. Doonan, H. Furukawa, K. Oisaki and O. M. Yaghi, *J. Am. Chem. Soc.*, 2011, **133**, 11478–11481.
- S2. M. Garbarczyk, F. Grinberg, N. Nestle and W. Kuhn, *J. Polym. Sci., Part B: Polym. Phys.*, 2001, **39**, 2207–2216.
- S3. M. Garbarczyk, W. Kuhn, J. Klinowski and S. Jurga, *Polymer*, 2002, **43**, 3169–3172.
- S4. W. Kuhn, P. Barth, P. Denner and R. Müller, *Solid. state. nucl. Mag.*, 1996, **6**, 295–308.
- S5. M. Ding, A. Ghoufi and A. Szymczyk, *Desalination*, 2014, **343**, 48.
- S6. S. J. Lue, C. Chien and K. P. O. Mahesh, *J. Membr. Sci.*, 2011, **384**, 17.
- S7. A. Dutta, K. Koh, A. G. Wong-Foy and A. J. Matzger, *Angew. Chem. Int. Ed.*, 2015, **54**, 3983.
- S8. A. W. Schüttelkopf and D. M. F. van Aalten, *Acta Crystallogr. Sect. D.*, 2004, **60**, 1355–1363.
- S9. D. Van Der Spoel, E. Lindahl, B. Hess, G. Groenhof, A. E. Mark and H. J. C. Berendsen, *J. Comput. Chem.*, 2005, **26**, 1701.
- S10. D. Li, W. Hu, J. Zhang, H. Shi, Q. Chen, T. Sun, L. Liang and Q. Wang, *J. Phys. Chem. C*, 2015, **119**, 25559.
- S11. A. K. Malde, L. Zuo, M. Breeze, M. Stroet, D. Poger, P. C. Nair, C. Oostenbrink and A. E. Mark, *J. Chem. Theory Comput.* 2011, **7**, 4026.
- S12. T. Darden and D. York, *J. Chem. Phys.*, 1993, **98**, 10089.
- S13. K. Y. Jee and Y. T. Lee, *J. Membr. Sci.*, 2014, **456**, 1–10.
- S14. V. García, E. Pongrácz, E. Muurinen and R. L. Keiski, *Desalination*, 2009, **241**, 201–211.
- S15. S. Y. Li, R. Srivastava and R. S. Parnas, *J. Membr. Sci.*, 2010, **363**, 287–294.
- S16. E. El-Zanati, E. Abdel-Hakim, O. El-Ardi and M. Fahmy, *J. Membr. Sci.*, 2006, **280**, 278–283.
- S17. S. N. Liu, G. P. Liu, X. H. Zhao and W. Q. Jin, *J. Membr. Sci.*, 2013, **446**, 181–188.
- S18. G. P. Liu, D. Hou, F. J. Xiangli and W. Q. Jin, *Chin. J. Chem. Eng.*, 2011, **19**, 40–44.
- S19. J. Huang and M. M. Meagher, *J. Membr. Sci.*, 2001, **192**, 231–242.
- S20. A. Jonquieres and A. Fane, *J. Membr. Sci.*, 1997, **125**, 245–255.
- S21. Z. Dong, G. Liu, S. Liu, Z. Liu and W. Jin, *J. Membr. Sci.*, 2014, **450**, 38–47.

- S22. G. Liu, W. S. Huang, J. Shen, Q. Li, Y. H. Huang, W. Jin, K. R. Lee and J. Y. Lai, *J. Mater. Chem. A*, 2015, **3**, 4510–4521.
- S23. J. Niemistö, W. Kujawski and R. L. Keiski, *J. Membr. Sci.*, 2013, **434**, 55–64.
- S24. E. A. Fouad and X. Feng, *J. Membr. Sci.*, 2009, **339**, 120–125.
- S25. D. L. Vrana, M. M. Meagher, R. W. Hutkins and B. Duffield, *Sep. Sci. Technol.*, 1993, **28**, 2167–2178.
- S26. H. Zhou, Y. Su, X. Chen and Y. Wan, *Sep. Purif. Technol.*, 2011, **79**, 375–384.
- S27. L. T. P. Trinh, Y. J. Lee, H. J. Bae and H. J. Lee, *J. Ind. Eng. Chem.*, 2014, **20**, 2814–2818.
- S28. S. Liu, G. Liu, J. Shen and W. Jin, *Sep. Purif. Technol.*, 2014, **133**, 40–47.
- S29. N. Qureshi, M. M. Meagher and R. W. Hutkins, *J. Membr. Sci.* 1999, **158**, 115–125.
- S30. H. Fan, Q. Shi, H. Yan, S. Ji, J. Dong and G. Zhang, *Angew. Chem. Int. Ed.*, 2014, **53**, 5578–5582.
- S31. X. Liu, Y. Li, Y. Liu, G. Zhu, J. Liu and W. Yang, *J. Membr. Sci.*, 2011, **369**, 228–232.
- S32. X. Liu, Y. S. Li, G. Q. Zhu, Y. J. Ban, L. Y. Xu and W. S. Yang, *Angew. Chem. Int. Ed.*, 2011, **50**, 10636–10639.
- S33. S. F. Li, P. Qin, M. N. Karim and T. Tan, *Green. Chem.*, 2013, **15**, 2180–2190.
- S34. A. G. Fadeev, Y. A. Selinskaya, S. S. Kelley, M. M. Meagher, E. G. Litvinova, V. S. Khotimsky and V. V. Volkov, *J. Membr. Sci.*, 2001, **186**, 205–217.
- S35. I. L. Borisov, A. O. Malakhov, V. S. Khotimsky, E. G. Litvinova, E. S. Finkelshtein, N. V. Ushakov and V. V. Volkov, *J. Membr. Sci.*, 2014, **466**, 322–330.
- S36. H. Tan, Y. Wu, Y. Zhou, Z. Liu and T. Li, *J. Membr. Sci.*, 2014, **453**, 302–311.
- S37. D. Korelskiy, T. Leppäjärvi, H. Zhou, M. Grahn, J. Tanskanen and J. Hedlund, *J. Membr. Sci.*, 2013, **427**, 381–389.
- S38. M. Omidali, A. Raisi and A. Aroujalian, *Chem. Eng. Process.*, 2014, **77**, 22–29.
- S39. F. Liu, L. Liu and X. Feng, *Sep. Purif. Technol.*, 2005, **42**, 273–282.
- S40. E. J. Jeon, A. S. Kim and Y. T. Lee, *Desalin. Water. Treat.*, 2012, **48**, 17–26.
- S41. S. Heitmann, J. Krings, P. Kreis, A. Lennert, W. R. Pitner, A. Górak and M. M. Schulte, *Sep.*

Purif. Technol., 2012, **97**, 108–114.

S42. Y. Li, L. H. Wee, J. A. Martens and I. F. J. Vankelecom, *J. Mater. Chem. A*, 2014, **2**, 10034–10040.

S43. J. Li, S. Ji, G. Zhang and H. Guo, *Langmuir*, 2013, **29**, 8093–8102.

S44. H. Fan, N. Wang, S. Ji, H. Yan and G. Zhang, *J. Mater. Chem. A*, 2014, **2**, 20947–20957.

S45. K. Srinivasan, K. Palanivelu and A. N. Gopalakrishnan, *Chem. Eng. Sci.*, 2007, **62**, 2905–2914.